**2137-27**

**Joint ICTP-IAEA Advanced Workshop on Multi-Scale Modelling for Characterization and Basic Understanding of Radiation Damage Mechanisms in Materials**

*12 - 23 April 2010*

**Connection between modeling and experiments**

M. Victoria

*Nuclear Fusion Institute, Universidad Politecnica de Madrid*
*Spain*

**Joint ICTP-IAEA Advanced Workshop on Multi-Scale Modeling for Characterization and Basic Understanding of Radiation Damage Mechanisms in Materials, April 12-23, 2010**

# The experimental validation of radiation damage modeling: an "historical" perspective

## I. The early results and analysis
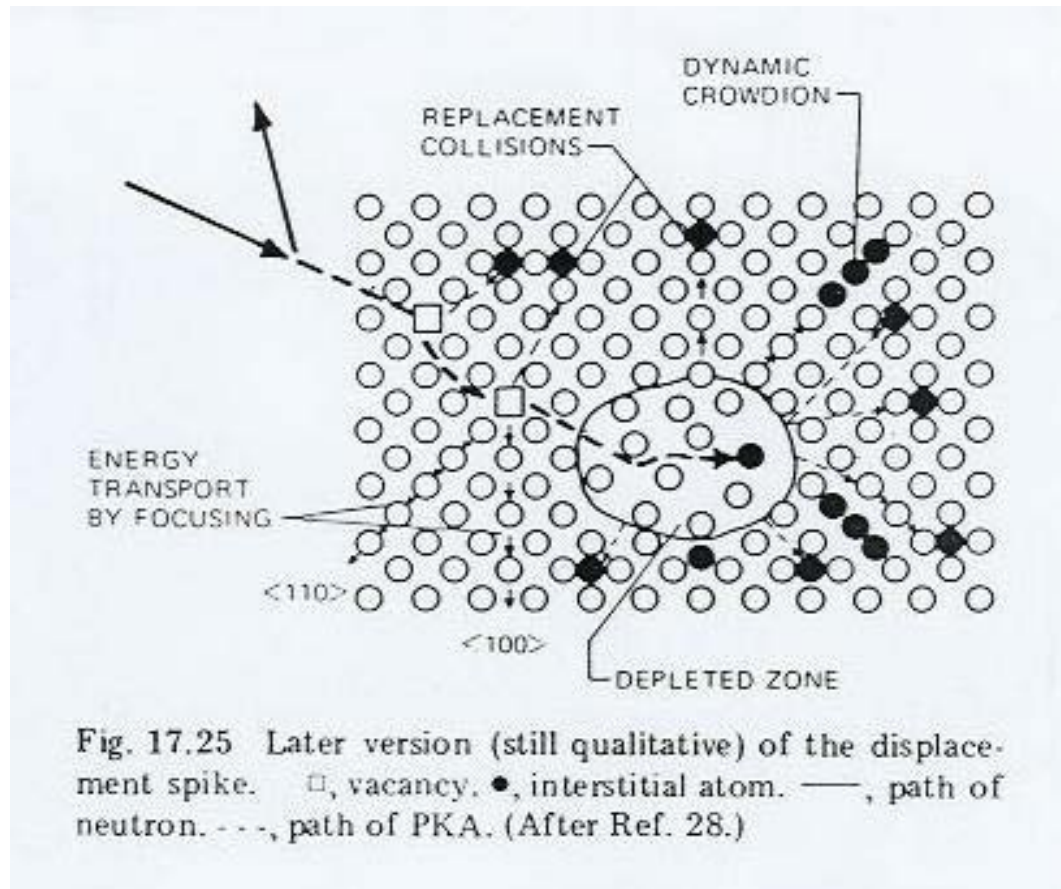
Max Victoria

Visiting Professor, UPM

## Acknowlegements

# Introduction

- Trying to understand the overall effects of radiation damage accumulation involves first a comprehension of its early stages, starting by the displacement process.

- The concept of a **displacement cascade** was first described by Seeger (1958) including the various defects formed and the formation of a depleted zone as propose by Brinkman (1954). Seitz and Kohler developed the idea of a **thermal spike** in the evolution of the cascade (1956), so already before 1960 (!!) a rather complete description of the displacement process was already available

- Atomistic numerical modeling came of age in the second half of the 80's with the development of the **embeded atom potential (EAM)** and its use in MD.

Fig. 17.25 Later version (still qualitative) of the displacement spike. □, vacancy. ●, interstitial atom. ——, path of neutron. - - -, path of PKA. (After Ref. 28.)

Seeger (1958)

- The developments have been much more slower on the experimental side, where spatial atomic resolution and time resolution of the order of picoseconds are needed.

- In this first lecture, we will discuss

(i) a charaterization of the irradiation with the different energetic particles available

(ii) the production of defects in radiation damage

(iii) The displacement cascade: modeling, experimental validation and observation of defects
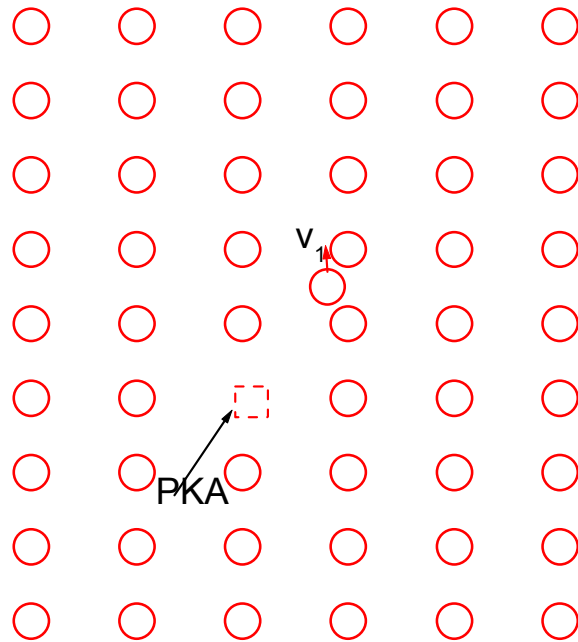
The formation of a Frenkel pair
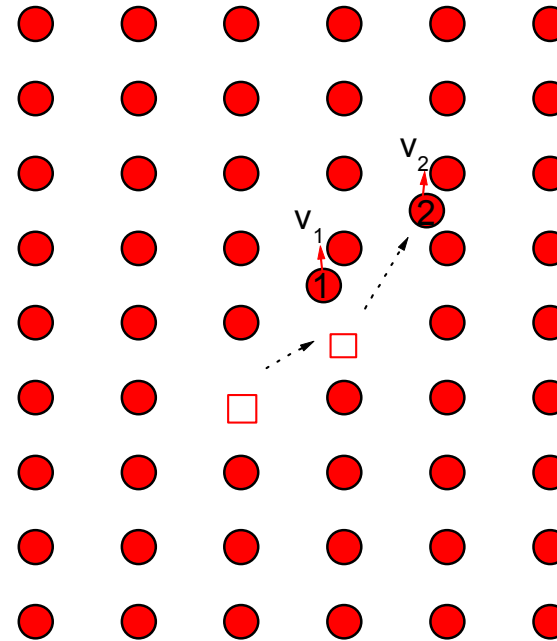
The initiation of the displacement cascade

# Deposition of energy

- As the metal is irradiated, the incoming particles loose their energy in the crystal through three types of processes:

- **Inelastic interactions** with target electrons, leading to ionization and/or excitations.

- **Elastic collisions** with the target (crystal) nuclei

- **Nuclear reactions**

$$\frac{dE}{dx} = \frac{dE}{dx}\bigg|_d + \frac{dE}{dx}\bigg|_e + \frac{dE}{dx}\bigg|_n$$
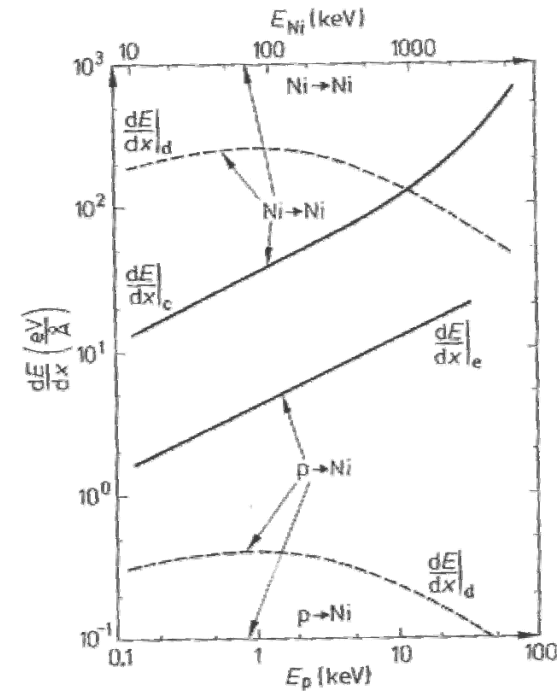


Figure 9-1. Electronic stopping $dE/dx|_e$ and nuclear stopping $dE/dx|_d$ as a function of particle energies $E_p$ and $E_{Ni}$ for protons and nickel ions, respectively, in Ni (calculated by the TRIM-code; Biersack and Haggmark, 1980). The energy scales are adjusted such that the reduced Lindhard energy $\varepsilon$ is the same for both particles.

Ullmaier

# (i) Electronic losses

For high energy particles, in the MeV range, the electronic stopping power is given by Bethe's formula:

$$\frac{dE}{dx}\Bigg)_e = \frac{2NeZ_1(M_1/m_e)}{E} \ln\left[\frac{4E}{(M_1/m_e)\,I_{avge}}\right]$$

Where N is the atom density of the target and $M_1$, $Z_1$ and E its mass, atomic number. $I_{avge}$ is an average ionization energy.

At low energies it is generally found:

$$\frac{dE}{dx}\Bigg)_e = kE^{1/2}$$

According to Lindhardt:

$$k = 0.3N\,Z^{2/3}$$

In the range

$$0 < E[keV] < 37Z^{7/3}$$

In **semiconductors and insulators** the electronic losses can lead to damage (charge deposition). In metals, the perturbation relaxes rapidly and leads mainly to heat disipation.

For **swift heavy ions** at extremely high values of the electronic stopping (few thousand keV per Å), defect formation can be induced by high local electronic excitations

❖ At energies over a few eV, the incoming particle will displace one or more atoms of the target lattice, creating a vacancy-interstitial pair: **a Frenkel pair (FP)**.

❖ Increasing the number of projectiles (neutrons, ions…) will increase the number of FP's created. If the target is at finite temperatures, these defects will migrate.In a perfect crystal, it could be expected that after some time **(annealing)** they would recombine, restoring the crystal to its initial state.

# Radiation damage to metals:

## A. Projectile

mass $M_1$, energy $E_1$

(neutron, proton, heavy ion,…)

## A. Target

Regular periodic array of atoms of mass $M_2$, at rest.

-Initial collision is the **primary collision**

-Struck atom is the **primary knock-on atom (PKA)**

In the collision, **energy T** is transferred to the lattice atom

If $T > E_d$, the lattice atom is displaced, forming a vacancy-interstitial pair: a **Frenkel pair**

# Displacement of target atoms
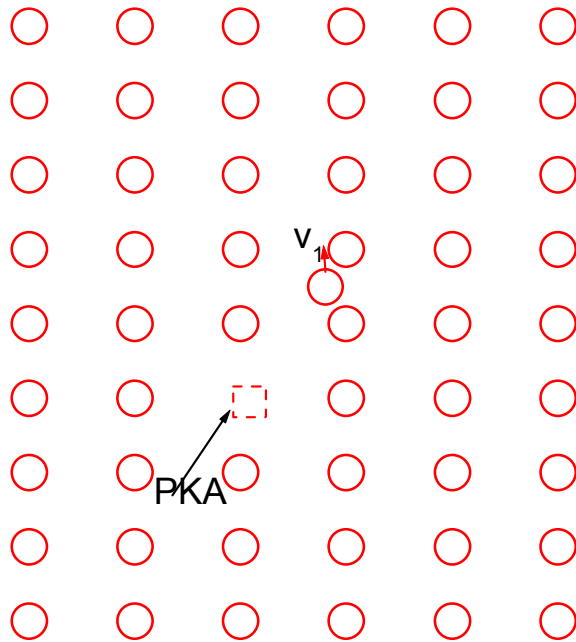


The formation of a Frenkel pair
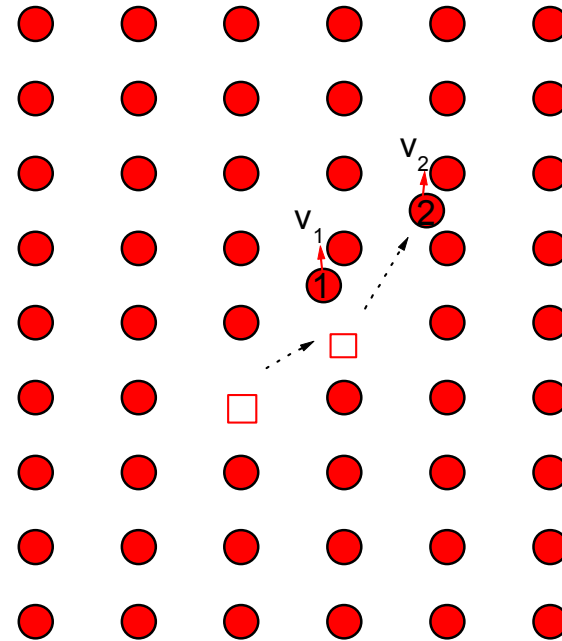
The initiation of the displacement cascade

# Energy of the primary event

Taking into account energy and momentum in the center of mass (CM) system, the maximum transfer of energy is:

$$T = T_{max} \sin^2 \Theta/2$$

and the (relativistic) for $T_{max}$ is :

$$T_{max} = 2 \frac{M_1 E_1 \left( E_1 + 2M_1 c^2 \right)}{\left( M_1 + M_2 \right)^2 + 2M_2 E_1}$$

Some typical values:

| Metal | $E_d$ [eV] |
|---|---|
| Pb, Al | 25 |
| Ti, Cu | 30 |
| Fe, Zr, Co | 40 |
| Ni, Cr, Mn, V | 40 |
| Mo, Nb | 60 |
| Ta, W | 90 |

For 1 MeV neutrons in non- relativistic approximation $(E \ll M_1 c^2)$

$$T_{max} = \frac{4M_1 M_2}{(M_1 + M_2)^2} E_1 = \frac{4\left(M_1 / M_2\right)}{\left(M_2 / M_1 + 1\right)^2} E_1$$

On a Fe target ($M_2 = A = 56$, $M_1 / M_2 \cong 56$), $T_{max} \cong 60$ keV

# Displacements produced by a PKA

The number of defects produced by a PKA can be calculated using the Kinchin-Pease model, which is a linear displacement model based in the following assumptions:

1. The displacements are produced by a series of independent two-body collisions between knock-on ions and stationary (lattice) atoms, triggered by the PKA.

2. The energy transfer in the collision is given by the hard sphere, isotropic scattering model.

3. The sequence of collisions stops after **n steps** when:

$$\mathbf{T/n < 2E_d}$$

The number of Frenkel pairs due to a PKA of energy T is:

$N_d = 0$      if   $T < E_d$

$N_d = 1$      if   $E_d \leq T \leq 2E_d$

$N_d = T/2E_d$  if   $T > 2E_d$

First correction: lower energy transfer are preferred so:

$$N_d(T) = \beta \, T/2E_d \qquad \beta \sim 0.8$$

Second correction: at higher energies (T > A [keV]), larger part of the energy is lost by transfer to electrons, so that the **damage energy** should be written:

$$E_D = T - Q$$

Where Q are the **inelastic losses**

# Deposition of energy

- A number of particles are available to be used in irradiations: electrons, protons, neutrons and ions

- We can expect a difference in behavior: they are not only very different in mass but we can also expect different types of interactions. For the charged particles is a Coulomb interaction, while the interaction of neutrons is well approximated by a hard collision model (beyond possible nuclear reactions).

- We define then a **primary recoil spectra** for a given energetic particle, that refers to the relative number of collisions in which an energy between T and T+dT is transferred from the primary recoil atom to other target atoms

The function

$$P(E,T) = \frac{1}{N} \int_{T_d}^{T} dT \frac{d\sigma(E,T)}{dT}$$

provides the fractional number of recoils between $T_d$ and T.
dσ/dT is the displacement cross section or the probability that a particle of energy E transfers a recoil energy T per unit dose and enrgy interval dT

For light ions dσ/dT α $(ET^2)^{-1}$ (Rutheford c.s.) where small energy transfers are favored. For neutrons dσ/dT almost constant

dσ/dT [barn/eV]
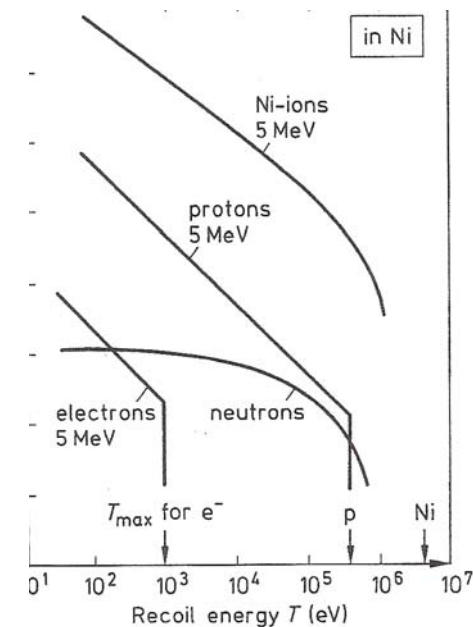


9-3. Differential cross section dσ/dT for trans-
a recoil energy T to nickel atoms as a function
r different irradiation particles.

# Weighted average recoil spectra

$$W(E,T) = \frac{1}{E_D(E)} \int_{T_d}^{T} dT \frac{d\sigma(E,T)}{dT} E_D(T)$$

ED is the damage energy created by a recoil of energy T (ED=T-Q) and

$$E_D(E) = \int_{T_d}^{T_{max}} dT \frac{d\sigma(E,T)}{dT} E_D(T)$$

$$T_{max} = \frac{4(M_1 M_2)}{(M_1 + M_2)^2} E$$

$$\frac{d\sigma_{coul}}{dT} dT = \frac{\pi M_1 (Z_1 Z_2 e^2)^2}{E} \frac{dT}{T^2}$$

$$\frac{d\sigma_{HS}}{dT} dT = A \frac{dT}{E}$$

Ignoring electron excitations, $E_D(T)=T$ and the integrations are

$$W_c = \frac{\ln T - \ln T_{min}}{\ln T_{max} - \ln T_{min}} \quad \text{Coulomb}$$

$$W_c = \frac{T^2 - T_{min}^2}{T_{max}^2} \quad \text{Hard sphere}$$

# Typical weighted recoil spectra
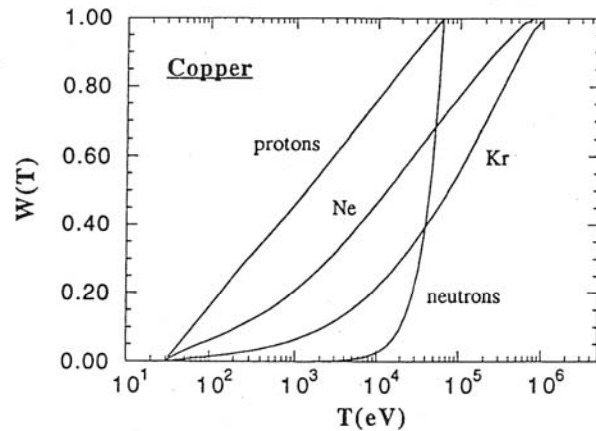


Fig. 3. Weighted recoil spectra for 1 MeV particles in Cu. Curves representing protons and neutrons (hard sphere), are calculated from Eq. (6a) and Eq. (6b), respectively. $W(T)$ for other particles, Ne and Kr, were calculated using Lindhard cross sections and include electronic excitation.

If we take the recoil energy up to which half of the displacements are produce $T_{1/2}$, it is 60 eV (~$2E_d$) for 5MeV $e^-$ and 60keV ($2000E_d$) for reactor n
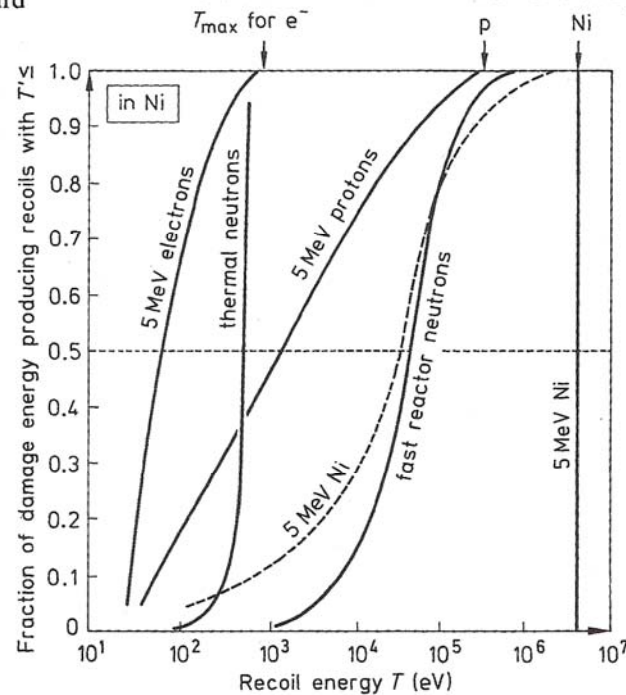


Figure 9-5. Fraction $W(T)$ of the damage energy producing recoils in nickel with $T'$ smaller than a given value $T$. For the self ion, Ni, two curves are shown: The solid line (step at 5 MeV) applies if the bombarding Ni-ion is considered as a PKA starting at the sample surface. The dotted curve is valid if energy transfers to Ni atoms excluding the bombarding Ni ion are considered.

# TRIM and Marlowe

These are binary collision codes that provide a good initial picture of the cascade

In **TRIM** (Ziegler and Biersack), the ion and target atom have a screened Coulomb during the collisions, including exchange and correlation interactions between the overlapping electron shells
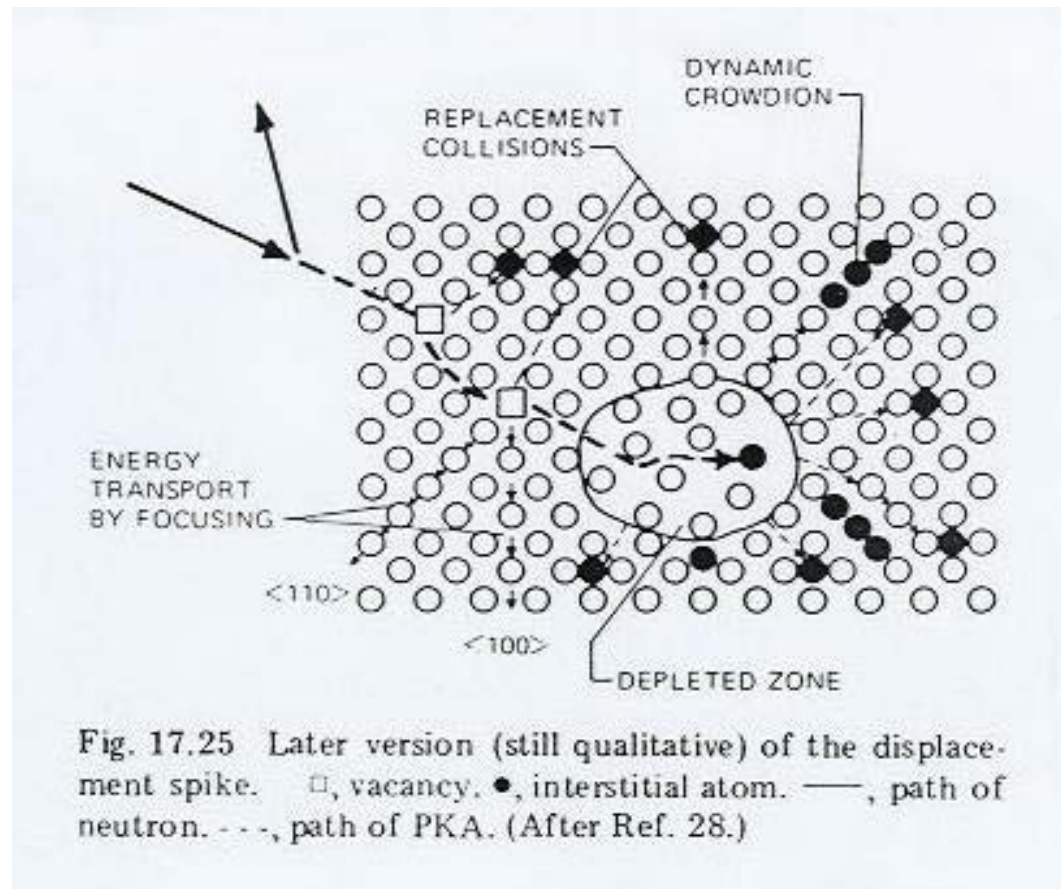
**MARLOWE** (Robinson) simulates atomic collisions in crystalline targets using the binary collision approximation and follows all moving atoms until they reach $E_d$

# Fe-implanted Fe (300 MeV)

# Fe-implanted Fe (300 KeV)

Fig. 17.25 Later version (still qualitative) of the displacement spike. □, vacancy. ●, interstitial atom. ——, path of neutron. - - -, path of PKA. (After Ref. 28.)
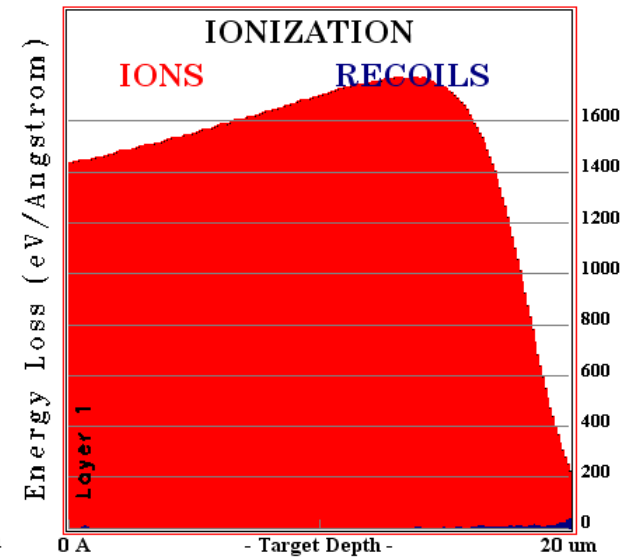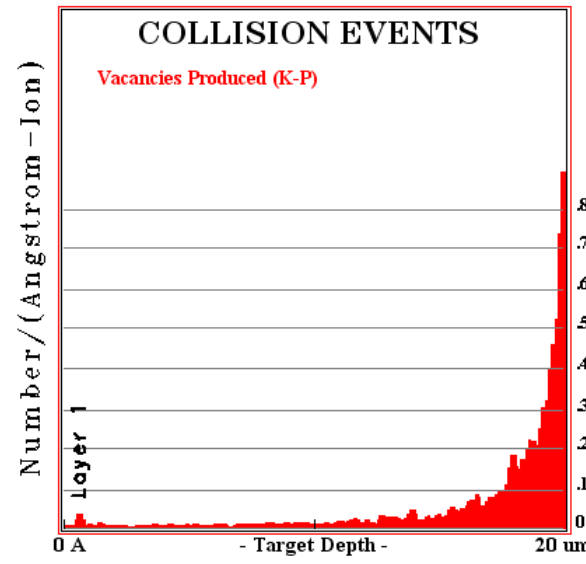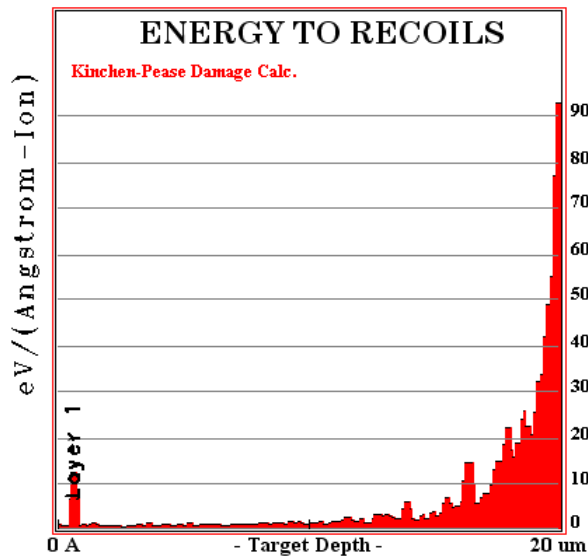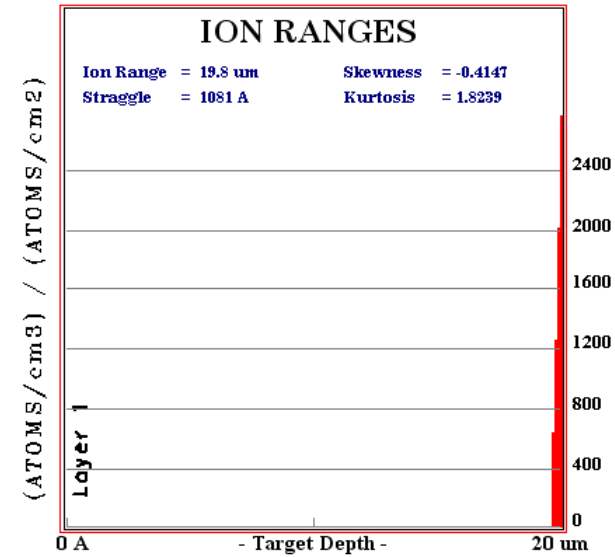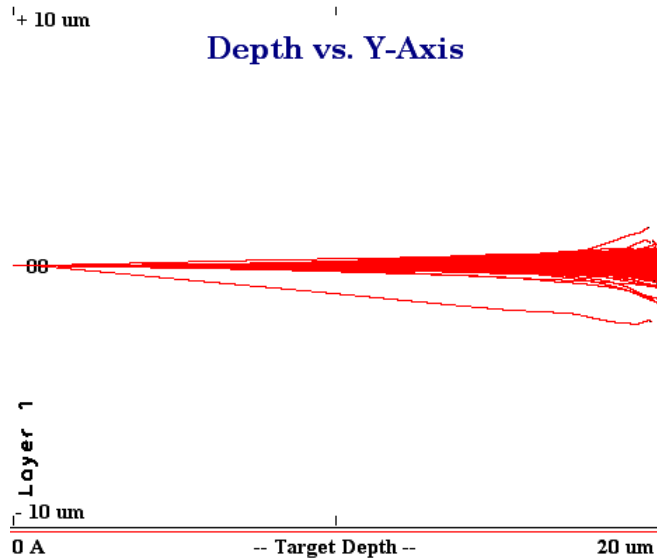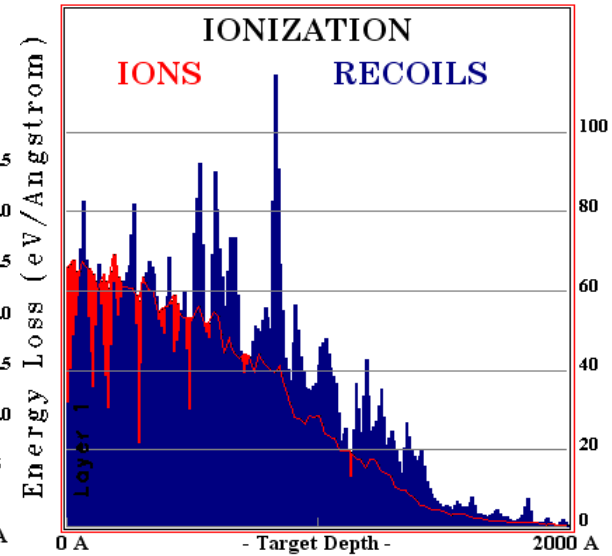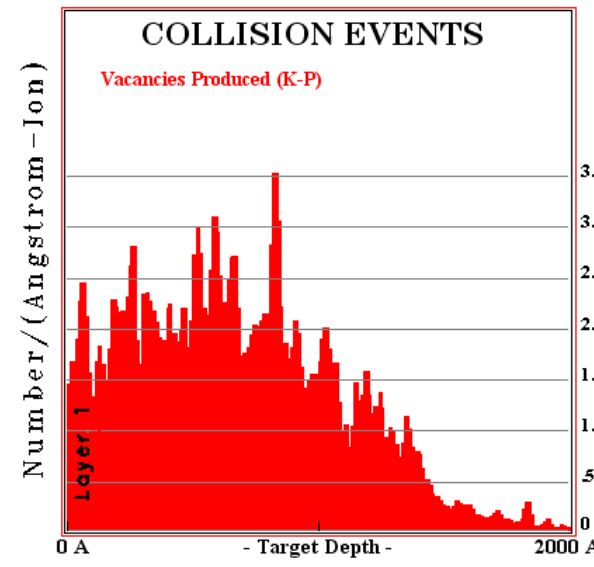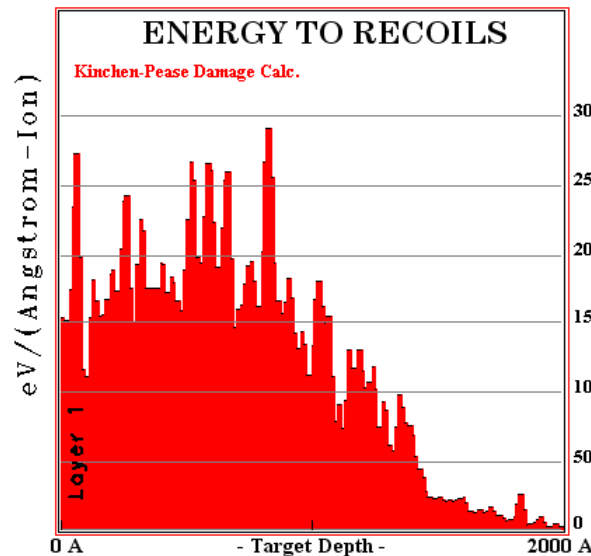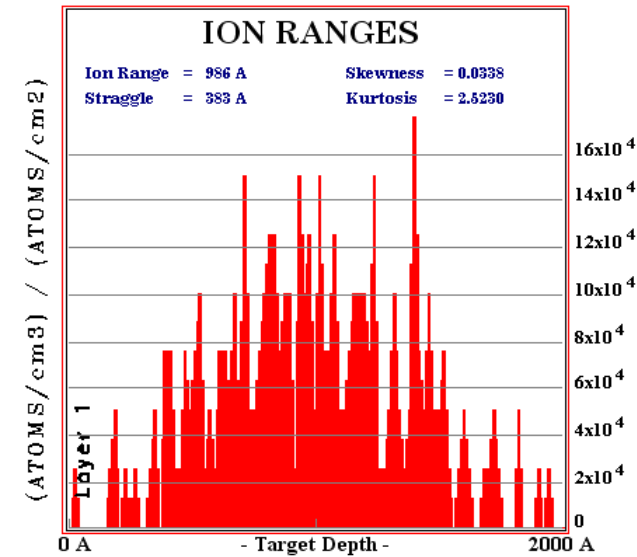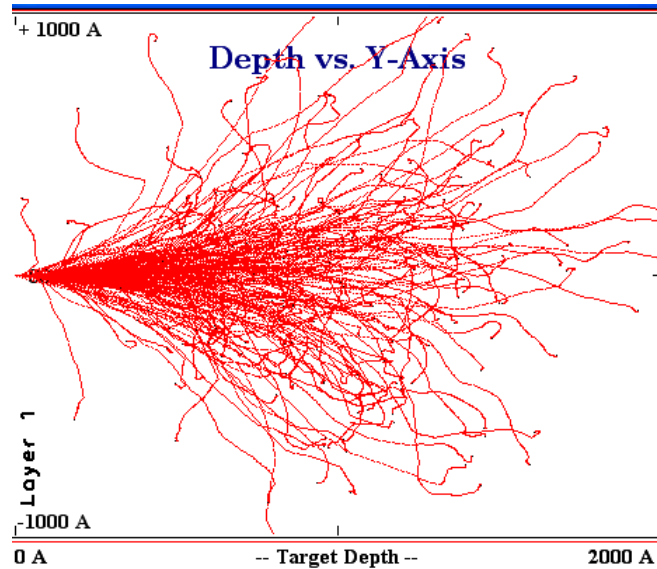
Seeger (1958)

# Cascade Evolution

1. Cu and Au
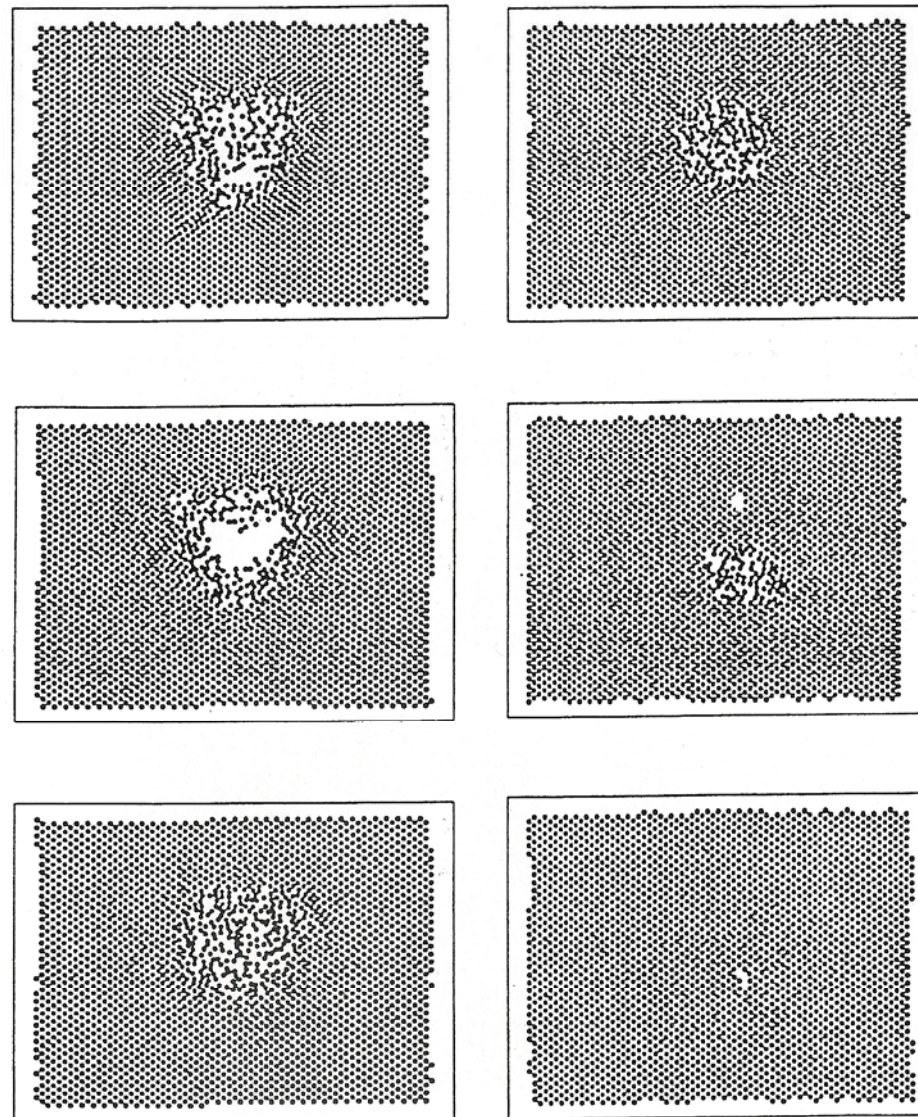
2. Au

# Cascade in fcc metals



35 ps

Cu 20keV ——> Cu

Au 20keV ——> Cu
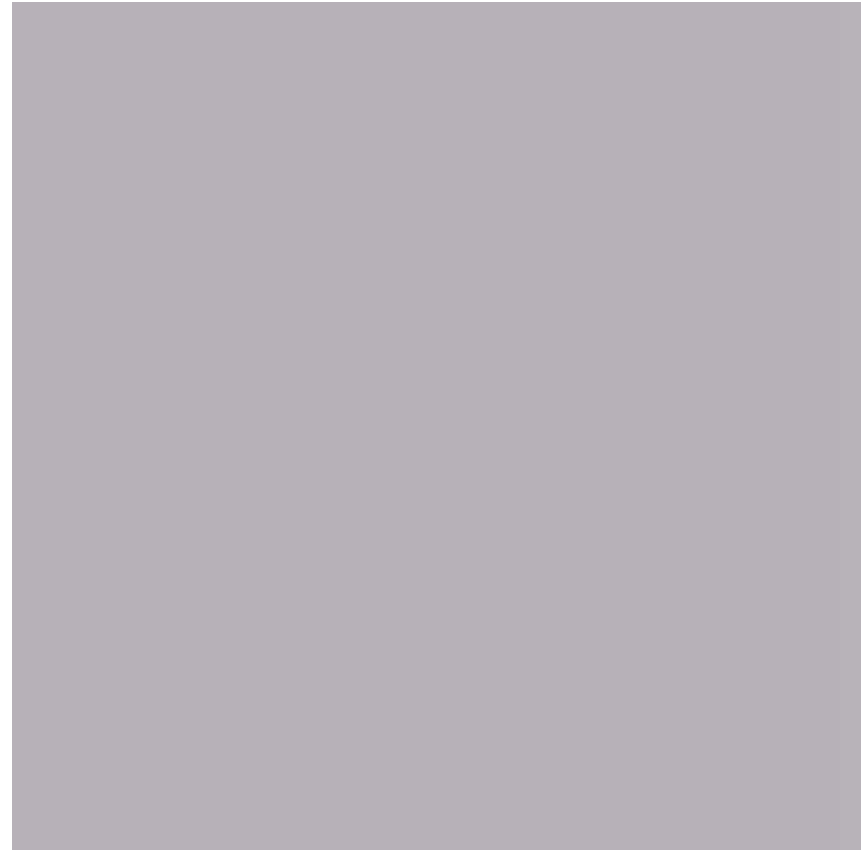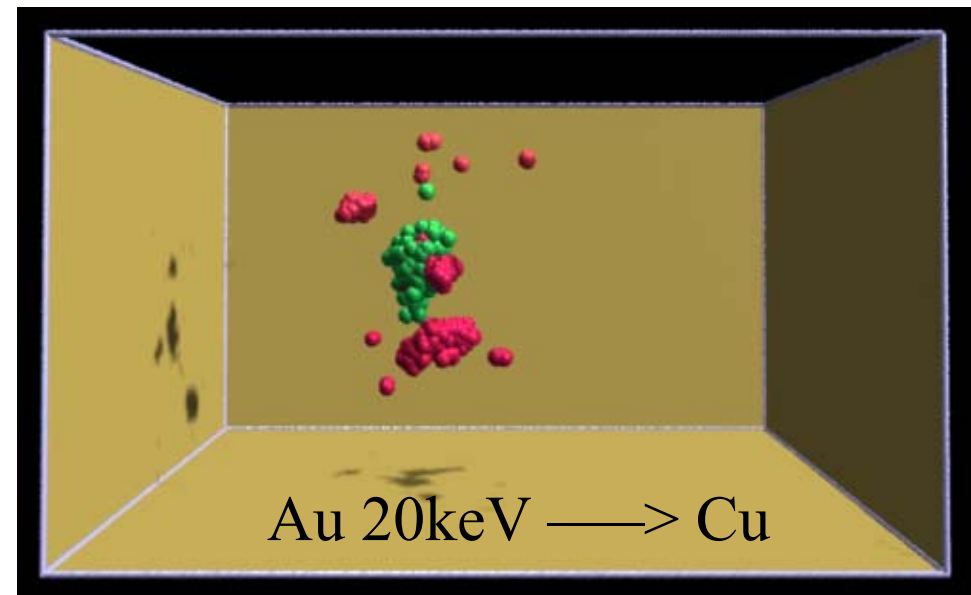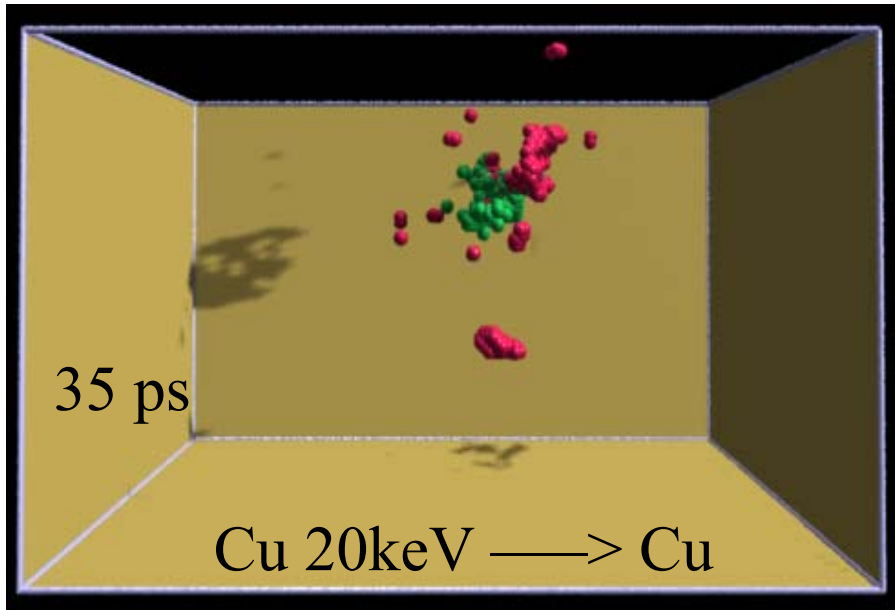
**F.C.C. materials (low stacking fault energy) result in the formation of both vacancy and interstitial clusters at the end of the collision cascade**

● Vacancies
● Interstitials

Pb 30KeV ——> Pb

Vacancies

Interstitials
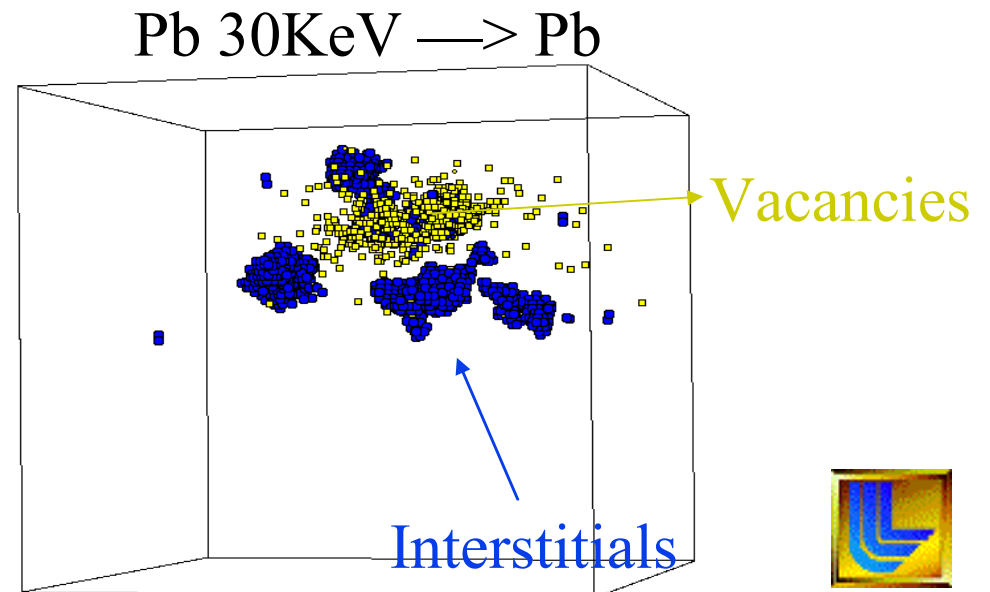
5. A series of snapshots of atoms in a 10 keV cascade in Au within a cross sectional slab of thickness $a_0/2$, viewed in the $\langle 100 \rangle$ ction. Each snapshot shows a different instant of time: (a) 0.62 ps, (b) 3.3 ps, (c) 5.0 ps, (d) 11.5 ps, (e) 17.7 ps, (f) 23 ps (from . [11]).

# Example: 20 keV recoil of Cu in Cu
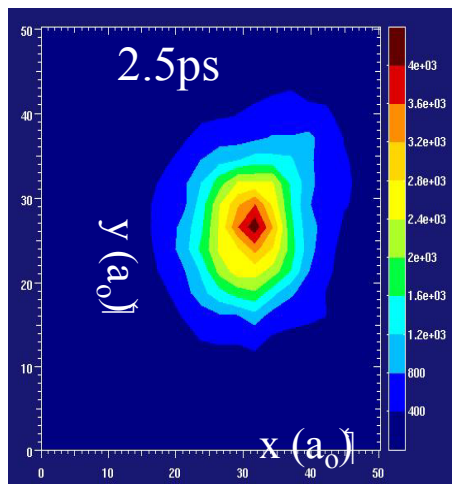
**Vacancy clusters generated by a cascade**


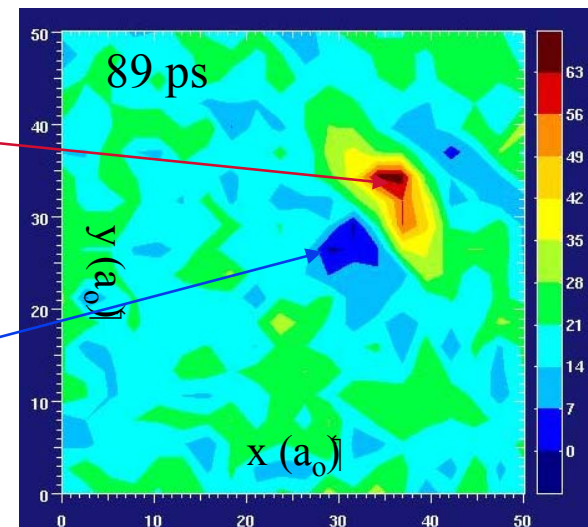
Vacancies

Interstitials

20 keV Cu in Cu

Vacancy cluster
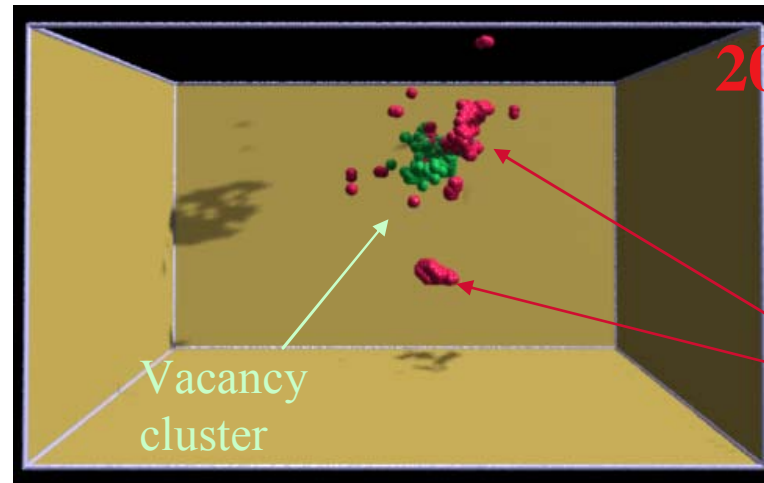
Interstitial clusters

Temperatures ($\gg T_m$) at short time (ps)

Stress distribution



2.5ps

$y$ ($a_o$)

$x$ ($a_o$)

Temperature (K)



Cu 20keV on Cu at 1.5 ps (Maxi

Perfect crystal at

Box (6.4nm)

$g(r)$

$r$ (Å)
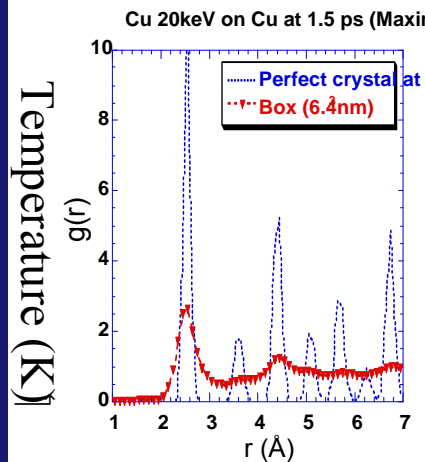
Compressive Stress

Tensile Stress



89 ps

$y$ ($a_o$)

$x$ ($a_o$)

Hydrostatic Stress (GPa)
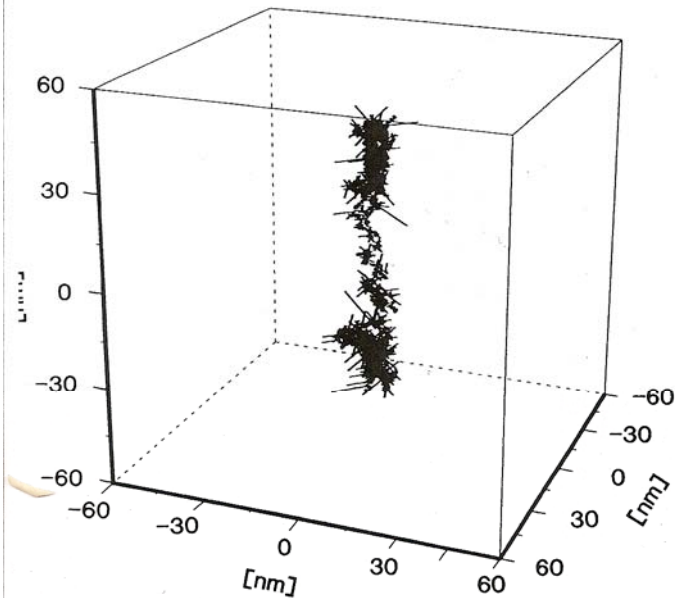
Fig. 1. 200 keV cascade in Ag. This is the output of the binary ollision code. Each dot represents an atom that has been set ito motion and that, at the end of the cascade, has an energy :ss than, but close to, the cut-off $E_c = 20$ eV. Replacement ollision sequences, as well as two subcascades, are clearly seen. Lengths are measured in nm.
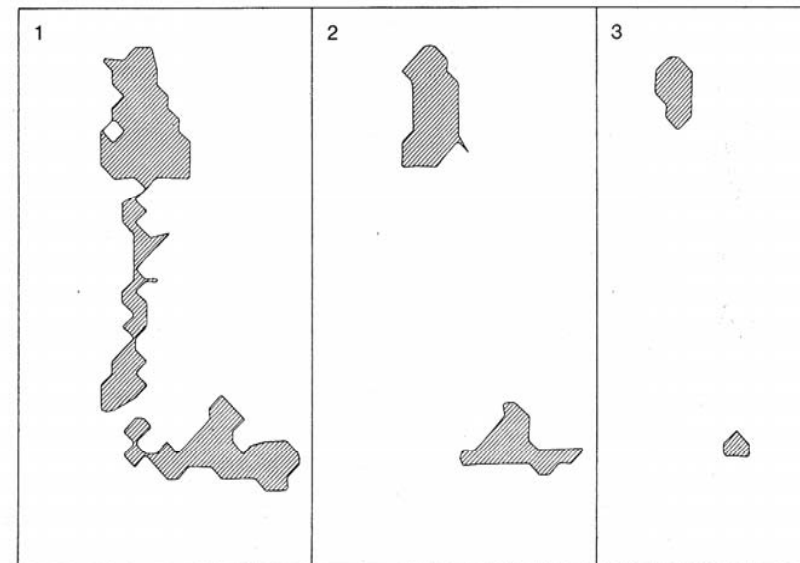
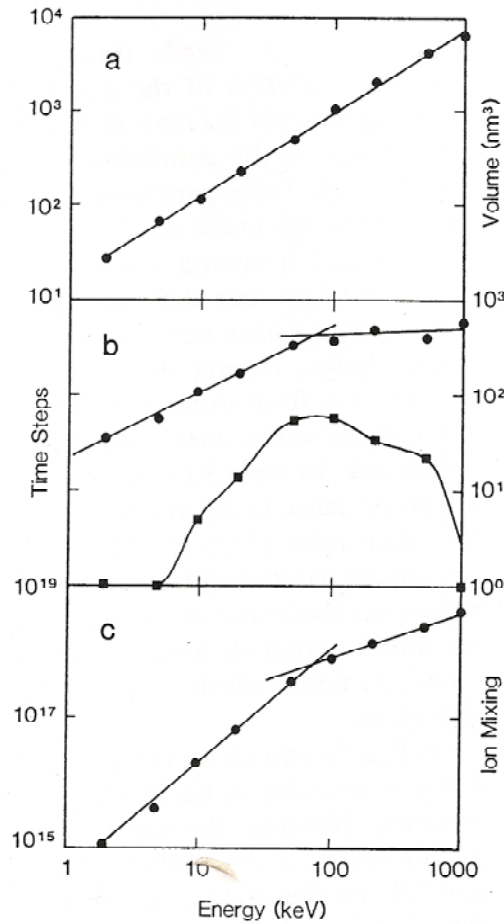Fig. 3. Two dimensional projections of the melt at three different times, corresponding to cascade in fig. 1.

Alurralde et al JNM (1990)

Fig. 7. Results for cascades in Ag; (a) maximum volume of the melt; (b) ●: lifetime of the liquid (straight lines are guides to the eye), ■: time at which the maximum volume of the melt appears; (c) ion mixing in units of $nm^2$ step/s.
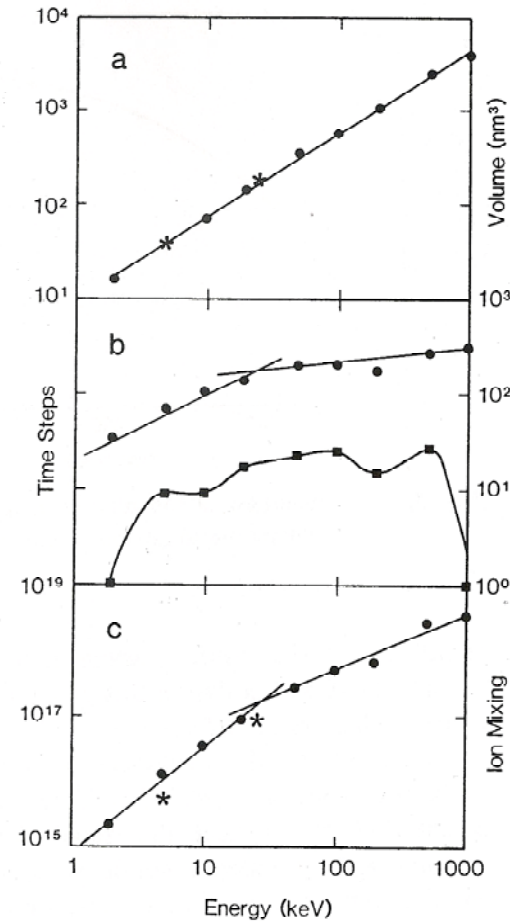
Fig. 8. Results for cascades in Cu; (a) maximum volume of the melt; (b) ●: lifetime of the liquid (straight lines are guides to the eye), ■: time at which the maximum volume of the melt appears; (c) ion mixing in units of $nm^2$ step/s, ∗: molecular dynamics results [16].

Alurralde et al JNM (1990)
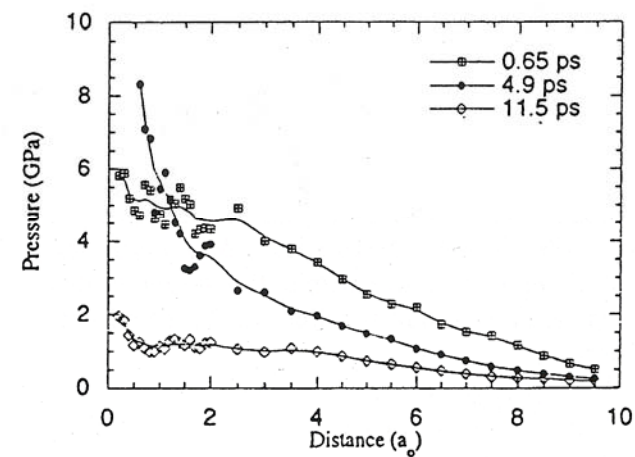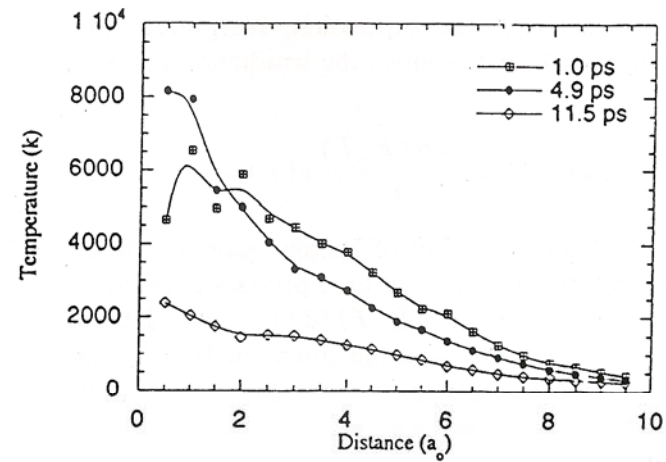
# Evolution of the displacement cascade



Fig. 7. (a) Temperature profile for the Au cascade shown in Fig. 5 (from Ref. [11]). (b) Pressure profile for the Au cascade shown in Fig. 5 (from Ref. [11]). $a_0$ is the lattice parameter.
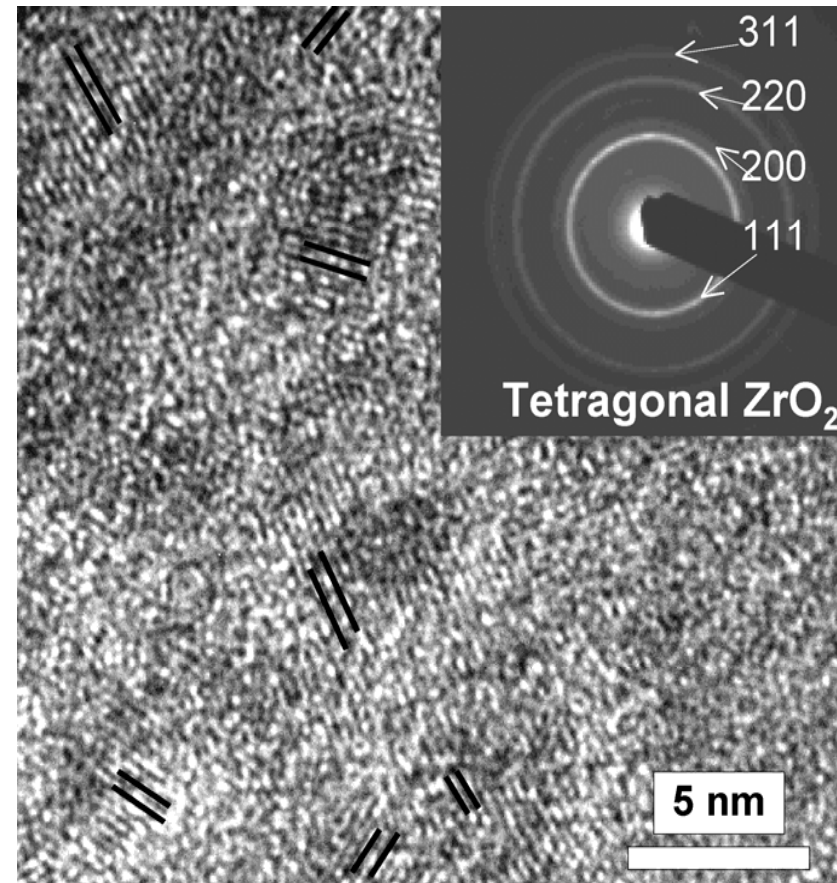
Averback (1994)

# Validation of cascade simulation: nanoscale melting

Non equilibrium nano-precipitates of $ZrO_2$ are observed in the $ZrO_2$-$SiO_2$ due to the fast cooling of the liquid droplet (cascade).
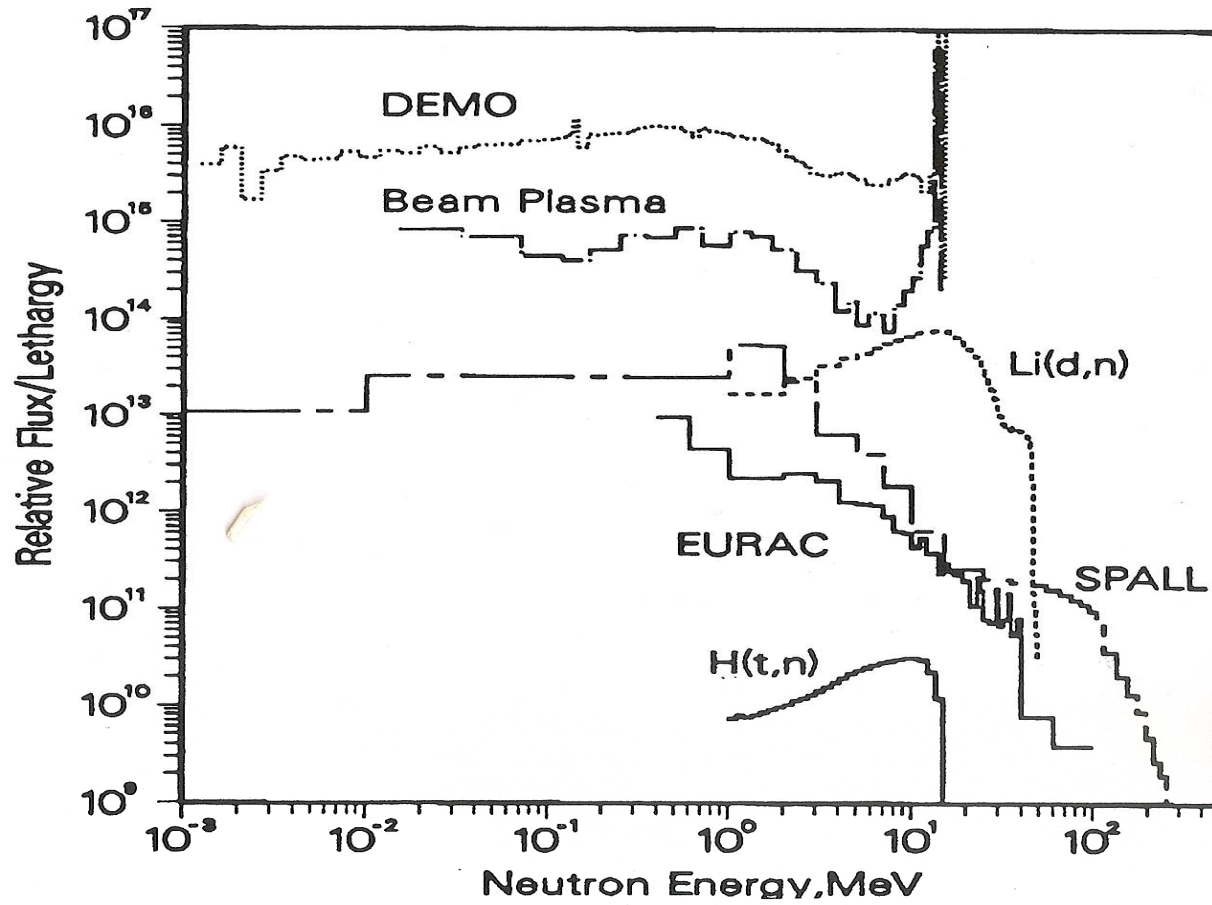
Zinkle et al., Nature 395 (1998) 56

Fig. 1. Comparison of neutron spectra; curves have been shifted arbitrary amounts for clarity.
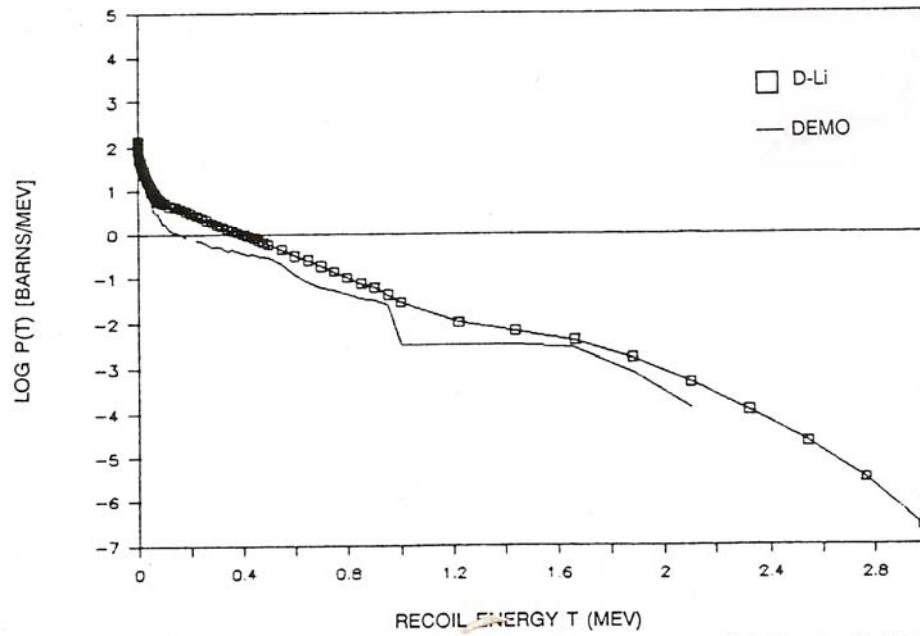
Doran (1990)

Fig. 3. Comparison of the iron PKA spectrum for the D–Li source (Pt. 2 at 8.5 cm) with that for the DEMO first wall.
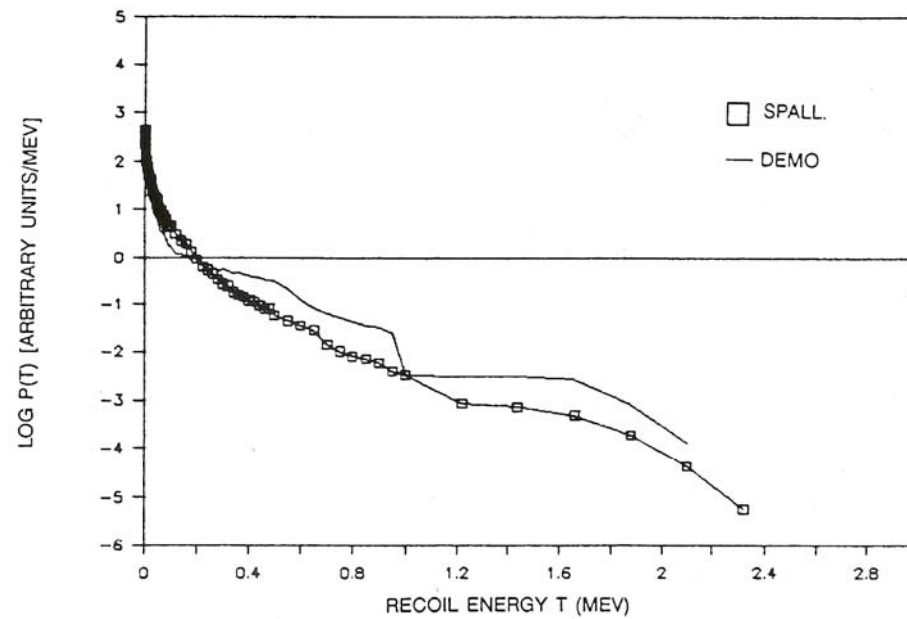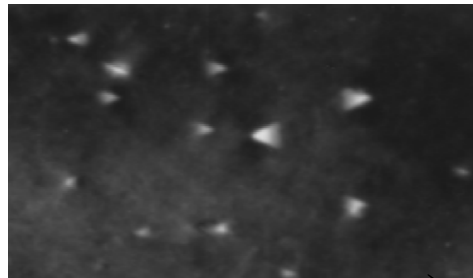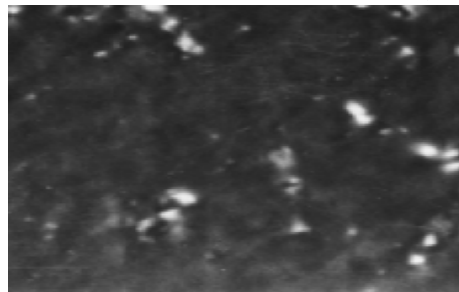
Doran (1990)



Fig. 6. Comparison of the iron PKA spectrum for Pepin's spallation source with that for the DEMO first wall.
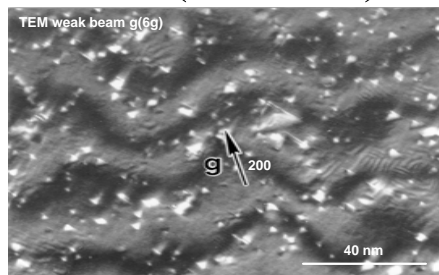
# Validation of cascade simulation: subcascade behavior
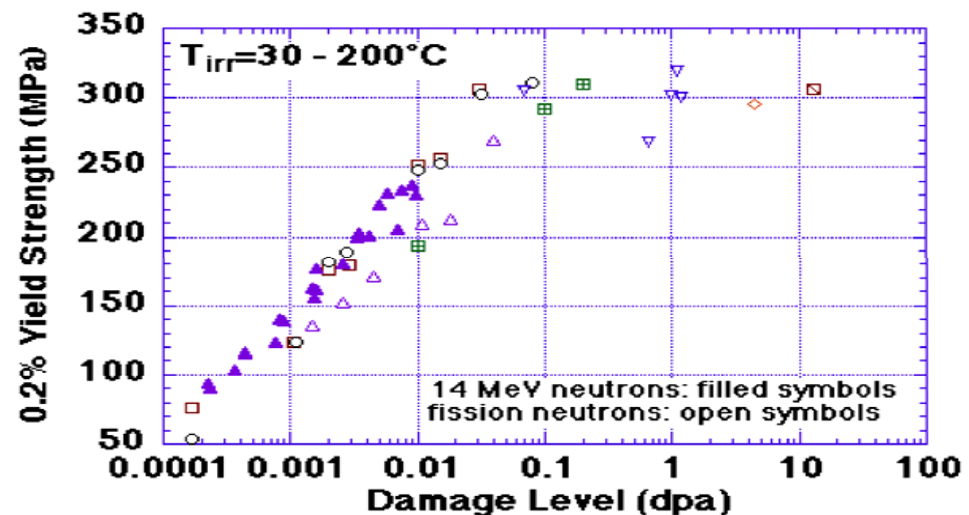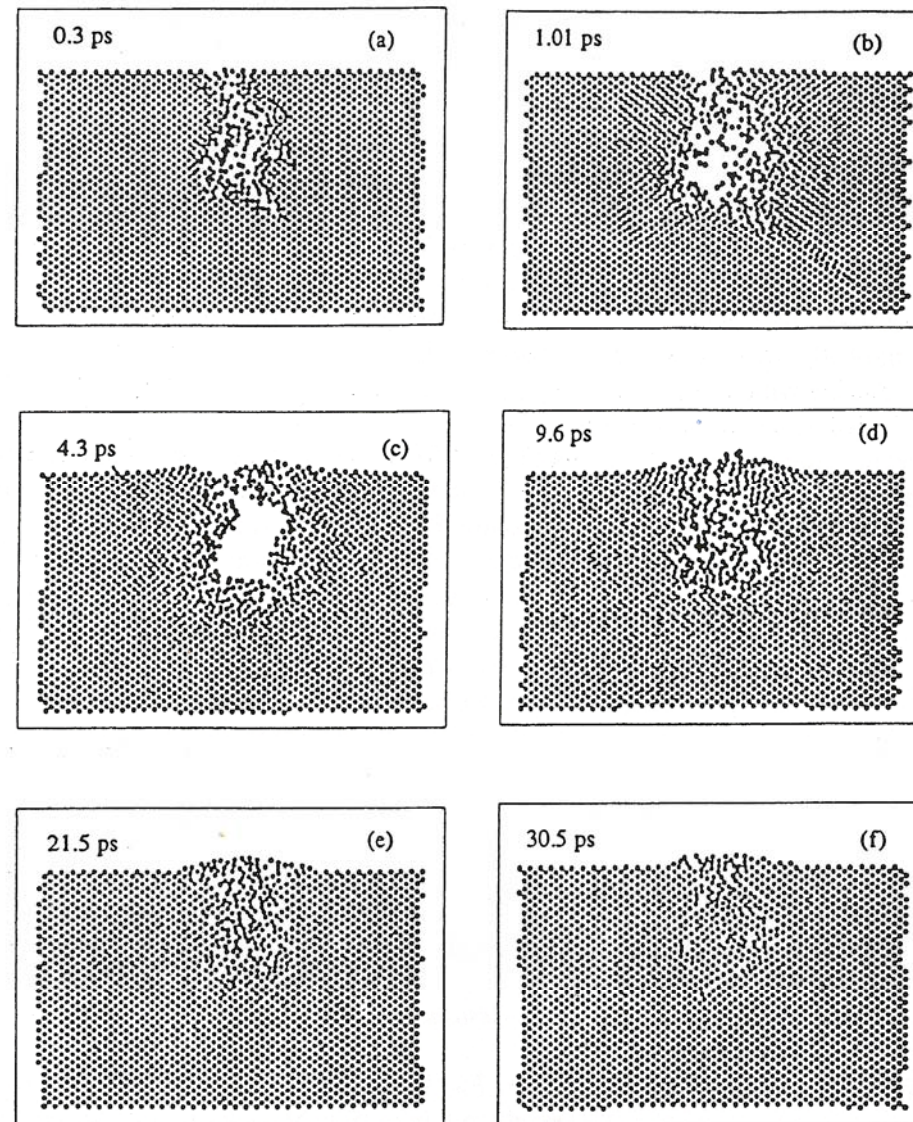


Fission (0.1-3 MeV)



Fusion (14 MeV)



590 MeV protons

Equivalency of damage

produced by fission and fusion

neutrons due to subcascade

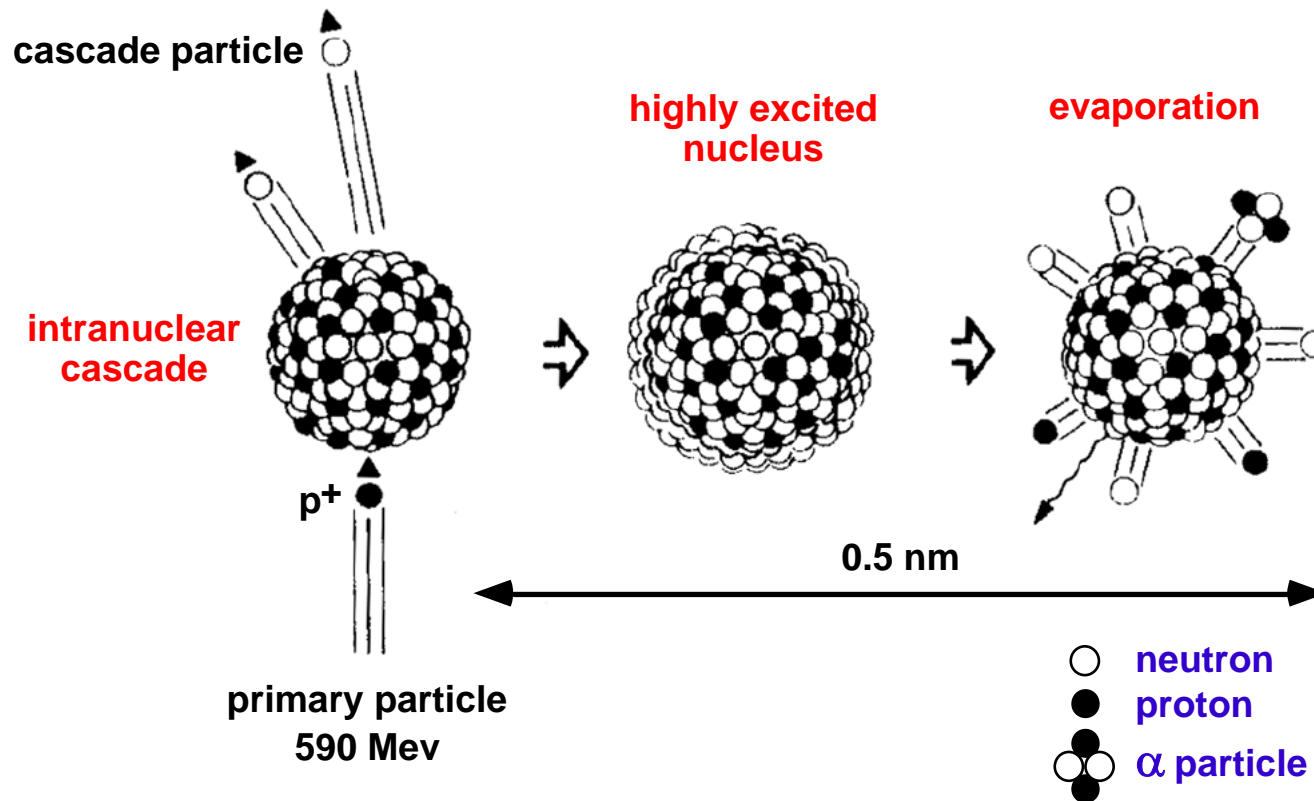formation (also valid for

other high

Nai Ghali et al (1994)

Fig. 10. Sequence of snapshots of the atomic positions within a cross sectional slab of thickness $a_0/2$ during 10 keV Au bombardment of Au (after Ref. [19]).

# Irradiation with 590 MeV Protons

## production of atomic displacements and impurities

# Swift heavy ions

If the energy of the incoming charged particle continues to increase into the region of hundred of MeV's and over, the electronic stopping becomes dominant, the stopping reaching >hundreds of keV per nm. The phenome observed is consistent with the formation of defects just by this electronic energy.
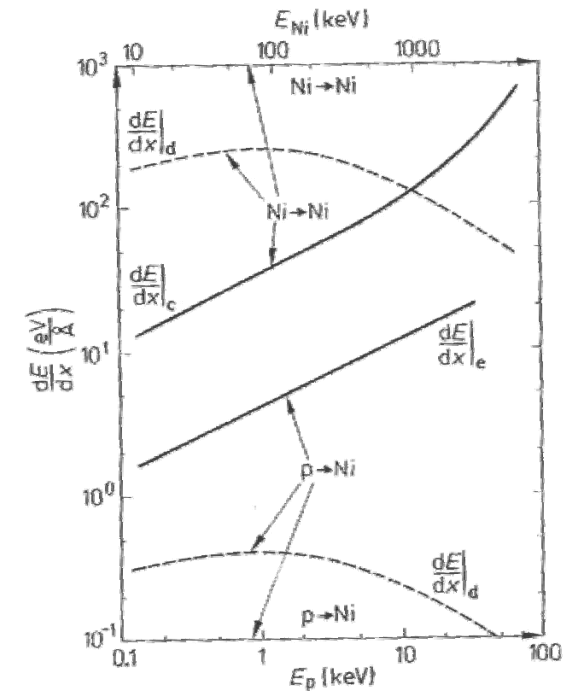


**Figure 9-1.** Electronic stopping $dE/dx|_e$ and nuclear stopping $dE/dx|_d$ as a function of particle energies $E_p$ and $E_{Ni}$ for protons and nickel ions, respectively, in Ni (calculated by the TRIM-code; Biersack and Haggmark, 1980). The energy scales are adjusted such that the reduced Lindhard energy $\varepsilon$ is the same for both particles.
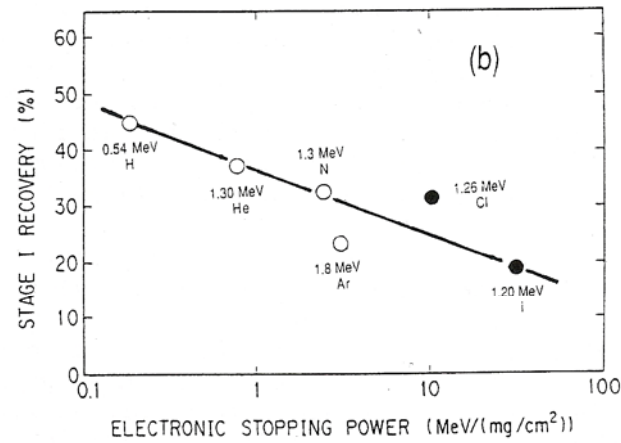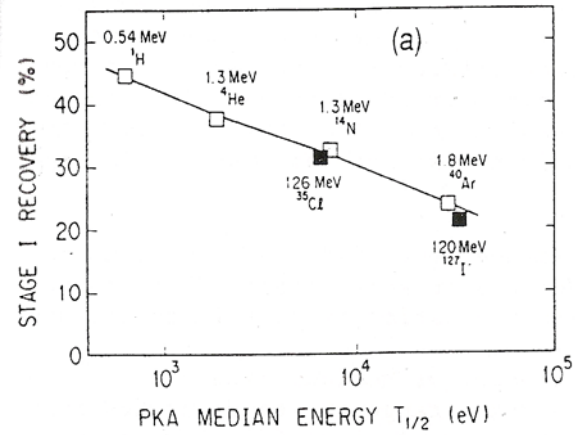
Figure 10 : Amount of stage-I recovery in copper after low energy (open squares) and high energy (solid squares) ion irradiations as a function of a) the median primary energy $T_{1/2}$ (see text) and b) the electronic stopping power. (redrawn from [22]).

See
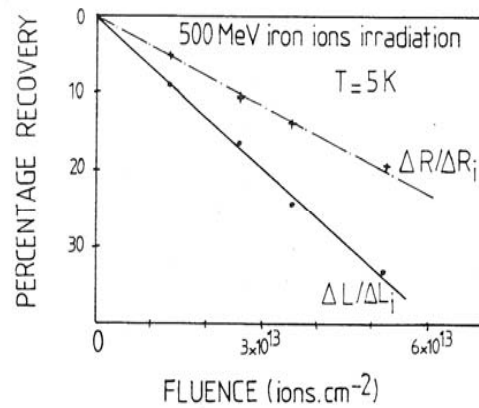N.Lazarev
this afternoon



A, Dunlop (1992)

Figure 11 : Relative electrical resistivity and length variations of an iron ribbon during an irradiation at 5 K with 500 MeV iron ions. This ribbon was first predoped with defects induced during low energy iron ions implantations (from [27]).
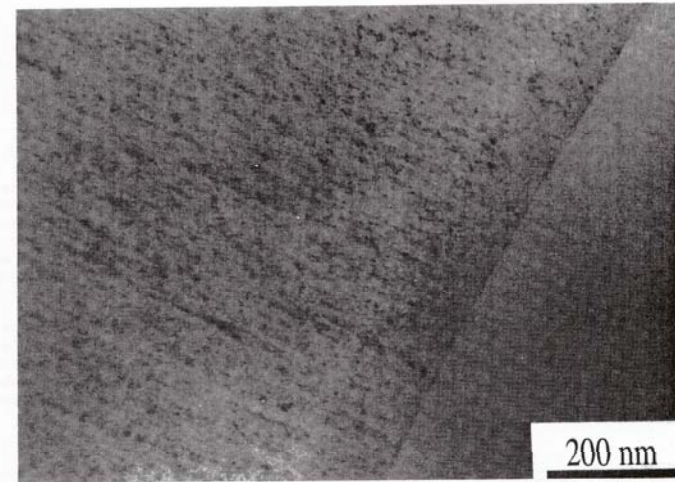


Figure 18 : Electron microscopy observation of titanium after irradiation with 4.5 GeV Pb ions up to a fluence of $2.4 \times 10^{13}$ ions/cm$^2$. Striated contrasts parallel to the ion beam direction under kinematical contrast condition at a tilt angle of 26° (from [36]).

| Time [ps] | Event | Result | Parameters |
|---|---|---|---|
| 10-6 | PKA: transfer of recoil energy | Lattice local disorder | $T_{PKA}$ $T_{dam}$ $d\sigma/dT$ |
| 10-6-0.2 | Formation of displacement cascade | Depleted zone (vacancies) Interstitial ejection | $N_d$ $n_{sc}$: avge. number of subcascades |
| 0.2- 3 | Spike formation and relaxation | Molten region Shock front Stable SIAs Atomic mixing | e-ph coupling Spike temperature Max. melt volume Max. melt lifetime |
| 3-10 | Core solidification and cooling | Vacancy collapse Disordered zone Amorphous zone | Atomic mixing efficiency |
| t> 10 | Thermal escape of interstitials and vacancies Reactions of the moving defects | Thermal escape of interstitials and vacancies Reactions of the moving defects | Irradiation temperature |

# The primary damage state

- Direct experimental confirmations ($T_{irr} < T_{stage\ I}$):

(i) Diffuse X-ray scattering of neutron irradiated Cu at 4.6 K, (Rauch et al.).

(ii) TEM in-beam observations in ion irradiated Cu at 20 K, (Kirk, Jenkins and Fukushima).

- Postirradiation (postmortem) observations

# Irradiation induced defect clusters in Cu (4.6 $10^{-2}$ dpa) and Pd (6.6 $10^{-2}$ dpa)